https://doi.org/10.1590/jatm.v16.1338 ORIGINAL PAPER

Performance Enhancement of a Variable Cross-Sectional Area Square Pipe Solar Heater

Noora A. Hashim[1,*], Rasha Hayder Hashim[1], Fatima Mohammed K. Al-Fatlwe[2], Sahib Shihab Ahmed[1]

1. University of Kufa – Engineering Faculty – Mechanical Engineering Department – Kufa – Iraq.
2. Al-Furat Al-Awsat Technical University – Engineering Technical College Najaf – Mechanical Engineering Techniques of Power – Najaf – Iraq.

***Correspondence author:** Nooraa.alkhalidi@uokufa.edu.iq

ABSTRACT

Recently, solar energy has become most favorable source of energy. It is sustainable and environmentally friendly, and one of the most common application of solar energy is the solar water heater, which has a wide commercial and domestic applications. To enhance the performance of this device, many modifications are recommended. The enhancements may involve changes in pipe shape or materials or in absorber plate manufacturing, or sometimes by using a thermal storage tank to maintain heating. In this study, a variable cross-sectional area pipe is used to enhance heat transfer. Firstly, the vertical length is increased at the outlet to 1.2-1.8 ratios, while the horizontal sides remain constant. Then, for the same ratio, the horizontal sides are varied while the vertical sides remain constant. Finally, both the vertical and horizontal sides are increase. A three-dimensional numerical analysis is used to investigate the conjugated heat transfer and the flow characteristics in the pipe under study for each case. FLUENT ANSYS 17.2 is used to achieve this analysis using finite volume technique. Energy, Navier-Stokes, and continuity equations are solved at constant heat flux condition for a range of Reynolds numbers from 100 to 500. The hydraulic-thermal function ε is adopted in this study. The best increase in ε is 48%, achieved in the case of changes to both vertical and horizontal dimensions at a ratio of 1.8. The lowest percentage of decrease in pressure drop is 9.7%, and the highest temperature difference found is and 45.5% for the same case when compared with the uniform case for Reynolds number of 100. The present work is validated with another study adopting Shah's empirical relation with a very good agreement.

Keywords: Solar energy; Solar water heater; Square pipe; hydraulic-thermal function; ANSYS.

INTRODUCTION

A Solar collector collects the incident solar radiation and transfers the absorbed heat to the fluid that flows through attached pipes. To insure that the heat transfers to the fluid with minimum losses, the heat transfer phenomena must be enhanced (Patel *et al.* 2005). Heat transfer enhancement is one of the essential tasks in most mechanical applications (Webb and Kim 2005). An appropriate improvement technique must be chosen, considering the cost and size of the arrangements (Massoud 2007). Two essential phenomena occur in the case of fluid flow in a pipe if it subjected to constant heat flux. They are the conjugated

Received: Mar 11 2024 | **Accepted:** May 24 2024
Section editor: Marcia Mantelli
Peer Review History: Single Blind Peer Review.

heat transfer and fluid friction. The latter causes pressure drop, velocity loss, and change in fluid temperature. Changing the tube, cross-sectional area has a significant effect on these two phenomena (Lee *et al.* 2013).

Many researches have studied this phenomenon experimentally, numerically, or analytically by solving of energy and flow equations. Vahidifar and Kahrom (2015) concluded experimentally that an increase in the convective heat transfer coefficient in any heat exchanger pipes can reduce the total heat exchanger size, weight, and as a result the cost. In their experiments, the enhancement was achieved by an electrical heat source (coil) located inside the pipe, which increased roughness and turbulence, resulting in a 128% enhancement in heat transfer. Negi *et al.* (2019) proved that the microchannel overall performance depended largely on Knudsen and Reynolds numbers. A computational fluid dynamics (CFD) analysis was conducted in order to simulate a counter microchannel flow under slip and no slip conditions. It was concluded that as Reynolds and Knudsen numbers increased, the pressure drop increased, so the effectiveness reduced. Bashir *et al.* (2019) deduced experimentally that the heat flux applied and the flow direction had no effect on the Nusselt number in the laminar regime. They also proved that the Nusselt number did not have a value of 4.36 for fully developed laminar flow in the range of Reynolds numbers larger than 1,000. Srivastava *et al.* (2017) used a constant heat flux convergent – divergent microchannel heat sink to investigate the channel thermal resistance, the friction coefficient, and the maximum temperature of substrate for a range of Reynolds number from 120 to 900, with and without ribs. It was found that using their configuration with cavities and ribs could reduce up to 40% in thermal resistance and the substrate temperature constant approximately. An increase in the Nusselt number of 15 to 40% was observed for the studied range of Reynolds numbers. However, their configuration poorly enhanced heat transfer, and its effectiveness gradually decreased in the case of high Reynolds numbers due to the high-pressure drop that occurred. Laila *et al.* (2021) adopted heat transfer model for a convergent-divergent rectangular channel. In their model, the governing equations were solved numerically in Cartesian coordinates. It was confirmed that the numerical solution was independent of slope direction (i.e., whether the channel area diverges or converges). Therefore, the solution achieved for the upper half was also considered for the lower part. It was concluded that the temperature profile decreased in the divergent flow and it increased in the convergent zone.

Salih and Yaseen (2021) carried out a two-dimensional laminar forced convection study of Al_2O_3-H_2O nanofluid flow in a circular pipe to analyze the fluid flow and the thermal behavior under constant heat flux conditions. The simulation achieved numerically with the aid of COMSOL software, the continuity, momentum, and energy were discretized and solved by the finite element method for Prandtl number = 5.42 and a range of Reynolds numbers ≤ 2,000. The results indicated that the use of Al_2O_3 nanoparticle enhanced the average heat convection coefficient by 10% for a volume fraction of 5%, with a maximum pressure drop of 15%. To validate their model, the empirical Shah equation was used and the results showed good agreement. Gheynan *et al.* (2019) studied the effects of nanoparticle concentration and diameter on the temperature fields of turbulent non-newtonian carboxymethylcellulose (CMC)/copper oxide (CuO) nanofluid in a three-dimensional microtube. Low- and high-Reynolds turbulent models were used in the modeling process. Interesting results were obtained, which can be helpful for engineers and researchers working on the cooling of electronic devices. A numerical investigation of water/Al_2O_3 nanofluid in a T-shaped enclosure with lid-driven by applying magnetic field was conducted by Toghraie (2017). For different values of Richardson, Hartmann numbers and void fraction. It was revealed that applying a magnetic field significantly effects the temperature domain (heat transfer) and fluid flow, considerably reducing the fluid's circulation mechanisms. Barnoon *et al.* (2019) investigated non-newtonian heat transfer and flow of nanofluid in a permeable enclosure with two cylinders embedded in the cavity with and without the thermal radiation effect. The study was conducted for different values of Rayleigh and Darcy numbers with different void fractions and cavity angle values. It was indicated that the changes in the cavity angle had a significant effect on heat transfer values.

In the present study, a three-dimensional analysis is conducted to simulate a water laminar flow in a variable cross-sectional area square pipe. The objective is to investigate the flow characteristics and heat transfer performance under a constant heat flux of 3,000 w·m^2 on the (top) wall. For values of Reynolds numbers ranging from 100 to 500 and different divergent ratios in vertical sides alone, horizontal sides alone, and in both two sides, the temperature difference and pressure drop through the pipe are calculated to display the effects of these two parameters on the thermal-hydraulic performance function ε.

The governing equations

A numerical investigation is conducted for a water flow in a square pipe of 1 m length, with an internal side length of 0.05 m and a thickness of 0.05 m, referred to as the square pipe case shown Fig. 1. Then the value of the vertical side increases at the outlet by a ratio of 1.2-1.8 for a constant value vertical side at the inlet. The horizontal sides then increase at the outlet in the second case for the same ratio range, and finally all sides are enlarged. The governing equations in each case are the continuity (Eq. 1), momentum (Eq. 2) and energy (Eq. 3) under the following assumptions:

- Forced convection, three-dimensional laminar steady state flow;
- Incompressible newtonian fluid;
- Body forces and viscous dissipation are ignored.

Continuity equation:

$$\nabla . \rho \vec{V} = 0 \tag{1}$$

Momentum equation:

$$\nabla . \left(\rho \vec{V} \vec{V}\right) = \nabla P + \nabla . (\mu \nabla^2 \vec{V}) \tag{2}$$

Energy equation:

$$\nabla . \left(\rho \vec{V} C_p T\right) = \nabla . (K \nabla T) \tag{3}$$

For the above three equations, the boundary conditions applied are no slip and uniform flow velocity at the inlet. Zero pressure at the outlet. The thermal conditions are constant inlet temperature and constant heat flux of 3,000 w·m^2 at the duct upper surface.

The Nusselt number is given by Eq. 4:

$$Nu_x = \frac{h_x D_h}{k_f} \tag{4}$$

where h_x is local heat transfer coefficient, which can be given shown by Eq 5:

$$h_x = \frac{q_x}{(T_w - T_b)} \tag{5}$$

Average coefficient of heat transfer is represented by Eq. 6:

$$h_{av} = \frac{1}{L} \int_0^L h_x dx \tag{6}$$

The hydraulic-thermal factor ε is given by Mashaei *et al.* (2012), as shown in Eq 7:

$$\varepsilon = \frac{h_{av}}{\triangle p^{1/3}} \tag{7}$$

where Δp is the pressure drop through the duct.

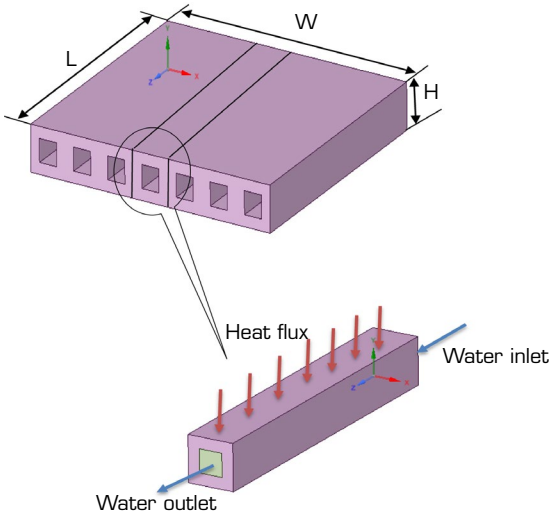

Source: ANSYS.

Figure 1. The square pipe geometry.

Test of grid dependency

To ensure accurate results for minimum grid size four mesh size are tested, which are 40 × 40 × 250, 40 × 40 × 350, 60 × 60 × 450, and 75 × 75 × 550 in x, y, and z directions. The used mesh is hexahedral unstructured type, as shown in Fig. 2. The selected mesh size is 60 × 60 × 450, which makes the more accurate results for the bulk temperature, as shown in Fig. 3. Also the selected mesh makes a maximum error of 0.48% if the values of Nusselt numbers from the model under study are compared with the results from the empirical Shah Eq. 8 (Kakac *et al.* 1987; Shah and London 1987), in the case of constant heat flux subjected to pipe of pure water inside flow at Reynolds number of 900. The result shows an excellent agreement as displayed in Fig. 4.

$$Nu_x = \begin{cases} 0.77\, X_*^{-1/3} & X_* \leq 0.01 \\ 3.657 + 6.874(10^3\, X_*)^{-0.488}\, e^{-57.2\, X_*} & X_* > 0.01 \end{cases} \quad (8)$$

where Nu_x given by eq. (4) and $X_* = \frac{x/D_h}{Re_{pr}}$.

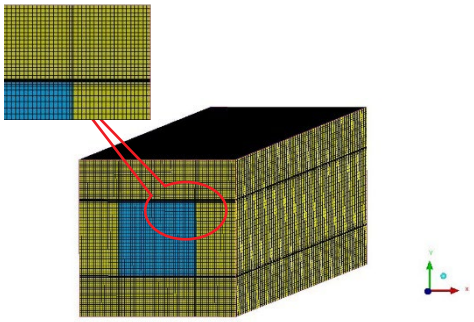

Source: ANSYS mesh.

Figure 2. The mesh generated for uniform duct case.

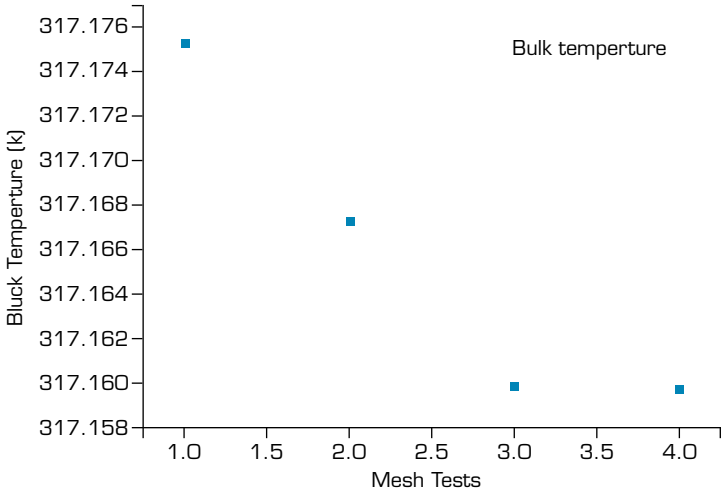

Source: ANSYS analysis.

Figure 3. Bulk temperature versus flow direction for different mesh sizes.

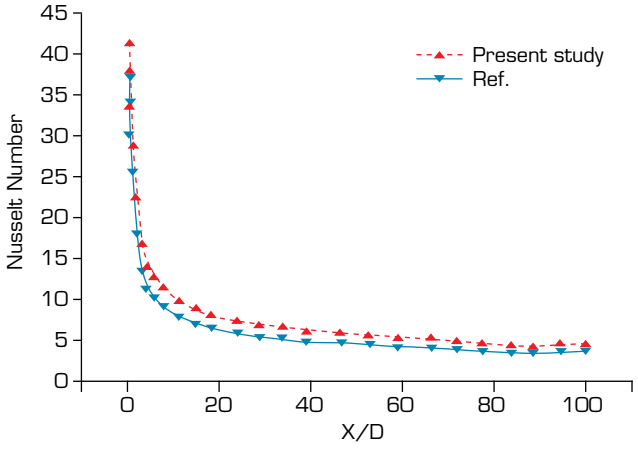

Source: ANSYS analysis.

Figure 4. A comparison between the studied model and the results from Shah equation for water flows inside a duct at Reynolds number of 900 and subjected to constant heat flux.

RESULTS AND DISCUSSION

By solving the computational model mentioned, many pressure and temperature contours can be obtained and the flow characteristics can be illustrated in the following figures for each case under study.

Temperature contours for different expansion ratios in the case of expanded vertical sides at the pipe exit are shown in Fig. 5. It can be observed that, as the expansion ratio increases, the temperature at the pipe exit increases, which means the heat transfer phenomena enhance. As the ratio increases, the pipe cross-sectional area increases, so the flow remains longer inside the tube and the convective heat transfer becomes more active. The maximum increase in temperature percentage is 7%. In Fig. 6 the pressure contours the same case above are shown for different expansion ratios. The pressure decreases as the ratio increases, which is a normal behavior; as the expansion ratio increases, the pressure forces are distributed over a larger area, so the pressure values decrease. The behavior in Figs. 7 and 8 is the same as in Figs. 5 and 6 for the horizontal sides increasing at the outlet with the same expansion ratios because the change in area is same. In Figs. 9 and 10, the expansion achieved in all sides, so the area is the larger

than in the previous two cases and the changes are more apparent. More significant increases in temperatures are achieved, which means there is a more enhancement in heat transfer phenomena.

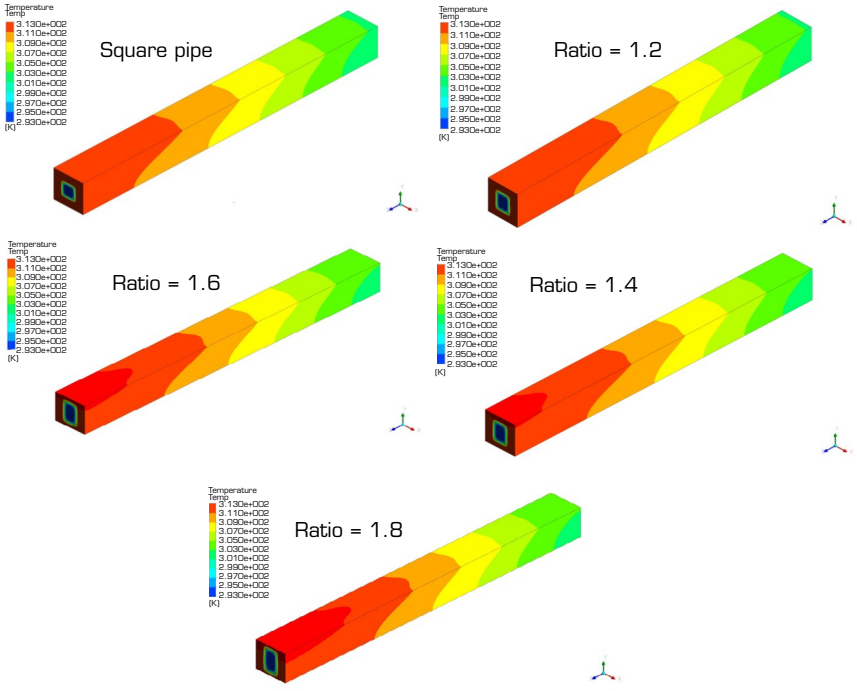

Source: ANSYS analysis.

Figure 5. Temperature contours in the case of expanded vertical sides at different expansion ratios.

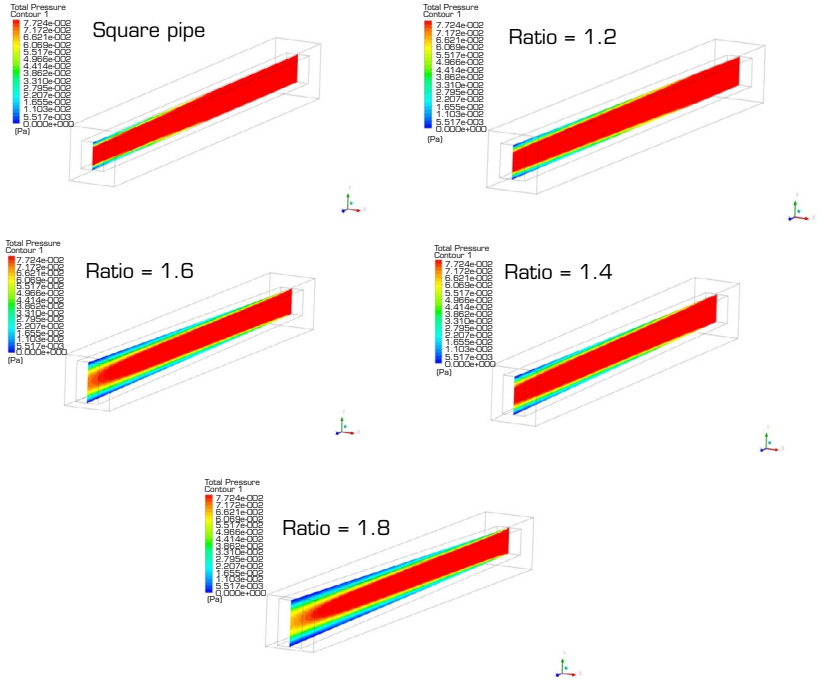

Source: ANSYS analysis.

Figure 6. Pressure contours in the case of expanded vertical sides at different expansion ratios.

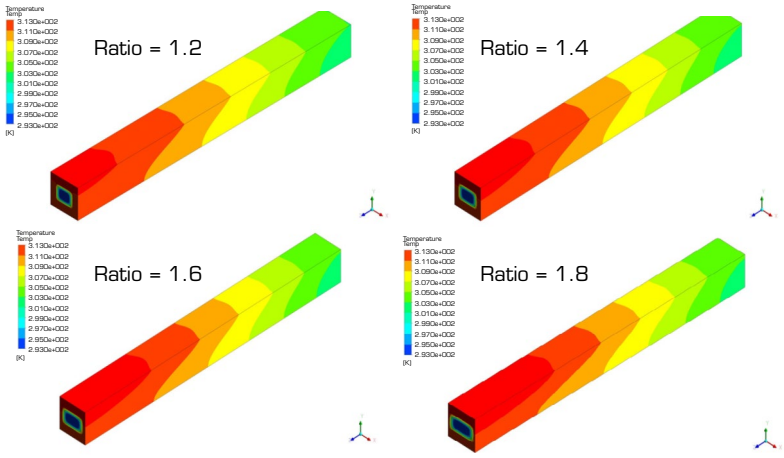

Source: ANSYS analysis.

Figure 7. Temperature contours in the case of expanded horizontal sides at different expansion ratios.

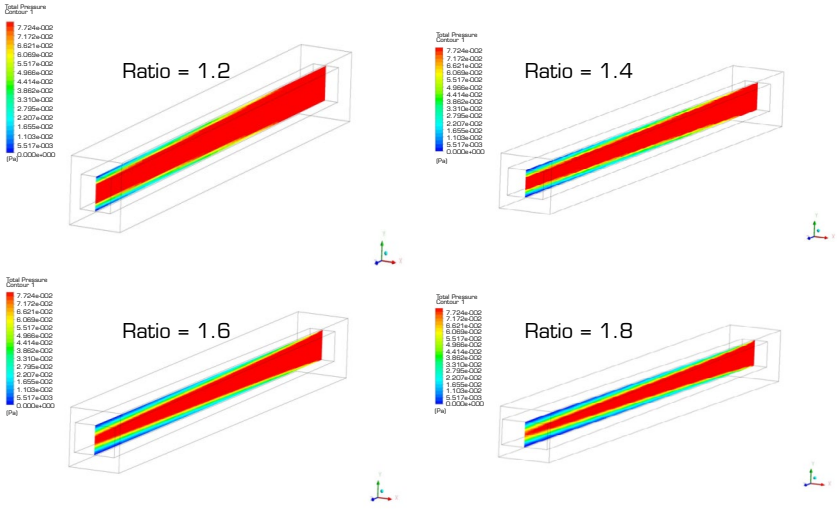

Source: ANSYS analysis.

Figure 8. Pressure contours in the case of expanded horizontal sides at different expansion ratios.

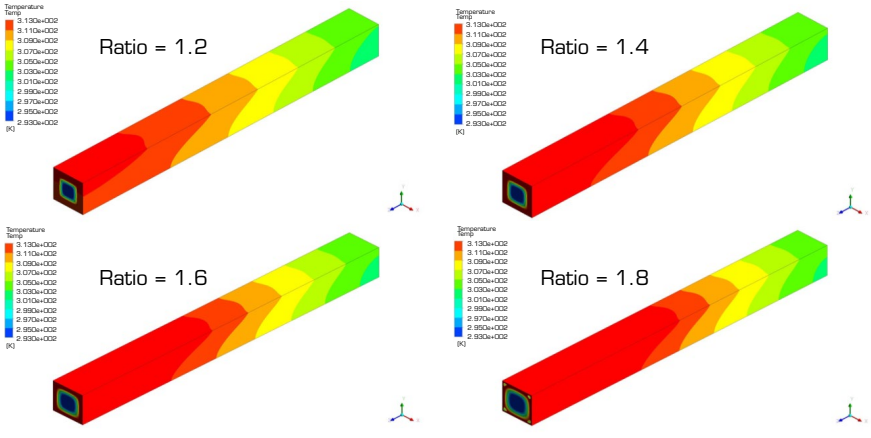

Source: ANSYS analysis.

Figure 9. Temperature contours in the case of all sides expanded at different expansion ratios.

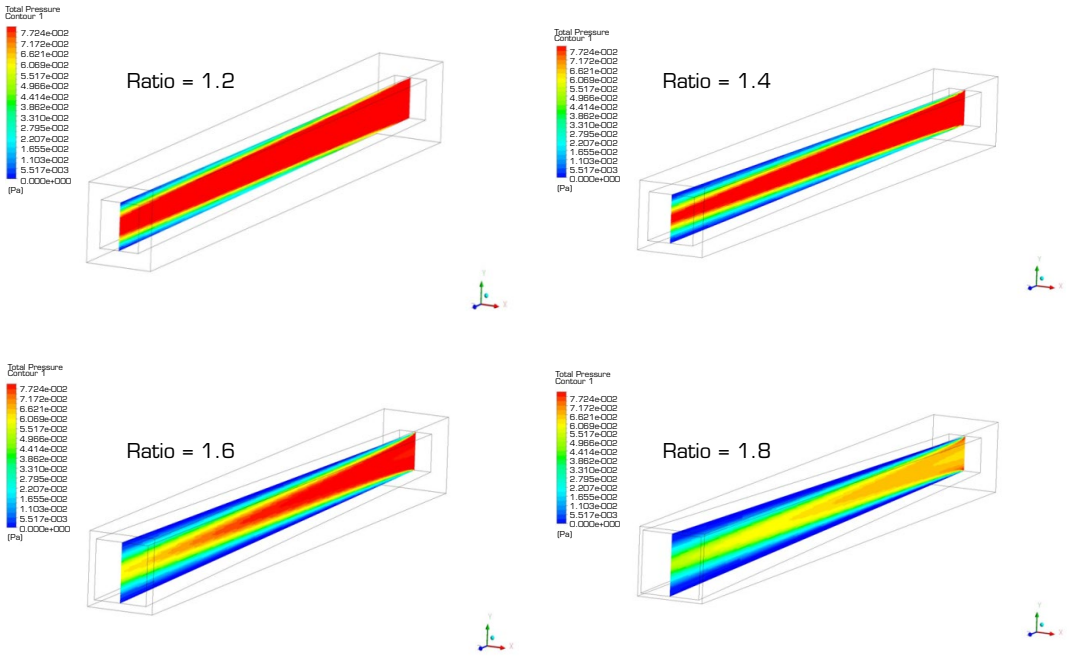

Source: ANSYS analysis.

Figure 10. Pressure contours in the case of all sides expanded at different expansion ratios.

Figures 11-13 show the temperature distributions along the flow direction for all cases under study. The temperature difference between the case of a 1.8 ratio and the square pipe reaches to 1.4 °C in the case of vertical side expansion at the pipe outlet. This value increases to 2.4 °C in the second case at the same ratio, as shown in Fig. 12. The maximum temperature difference of 9 °C (at the pipe exit between the case of a 1.8 ratio and the square pipe) occurs in the third case when all the pipe sides are expanded at the outlet. A large temperature difference was achieved due to the increase in area, as shown in Figs. 12 and 13.

Figures 14-16 illustrate the pressure drop through the flow direction for the three cases studied. In Fig. 14, the maximum pressure drop occurs in the case of the square pipe, and as the expansion ratio increases, the pressure drop values decrease until the enhancement reaches to 72% at a ratio of 1.8. The same enhancement ratio is obtained in the second case, as shown in Fig. 15 because the same change in area occurs. In the third case, the enhancement in pressure drop reaches to 153% at the same ratio because the area is doubled.

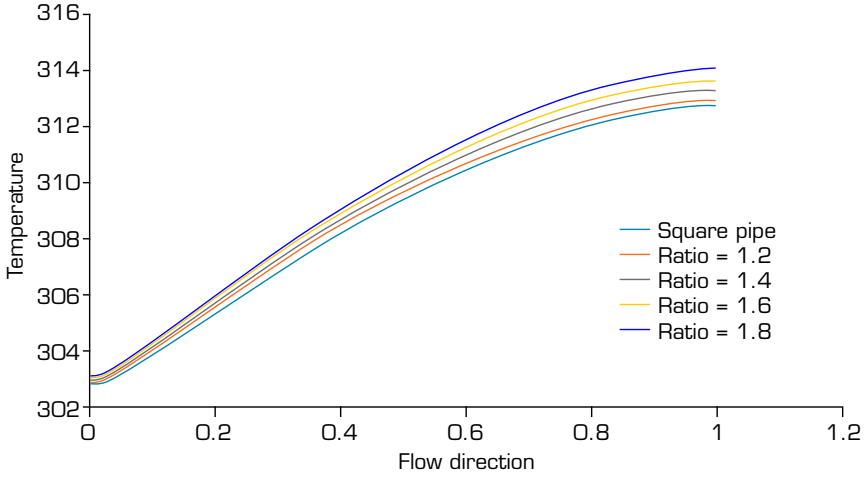

Source: ANSYS analysis.

Figure 11. Temperature distribution for different expansion ratios in the case of expanded vertical sides at the pipe exit.

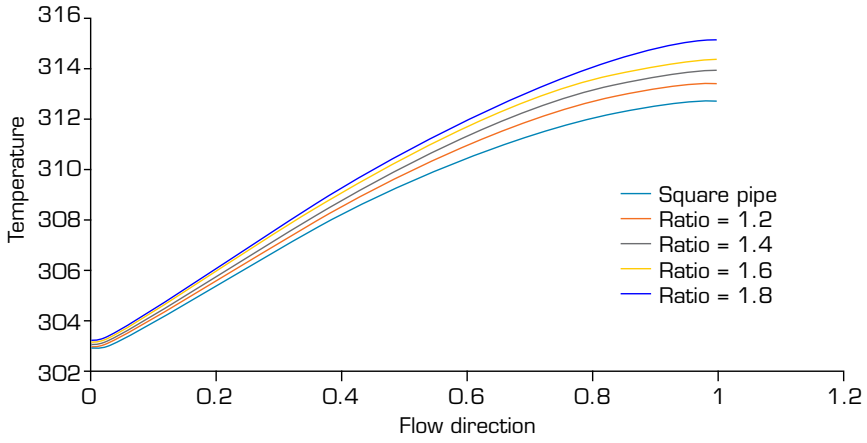

Source: ANSYS analysis.

Figure 12. Temperature distribution for different expansion ratios in the case of expanded horizontal sides.

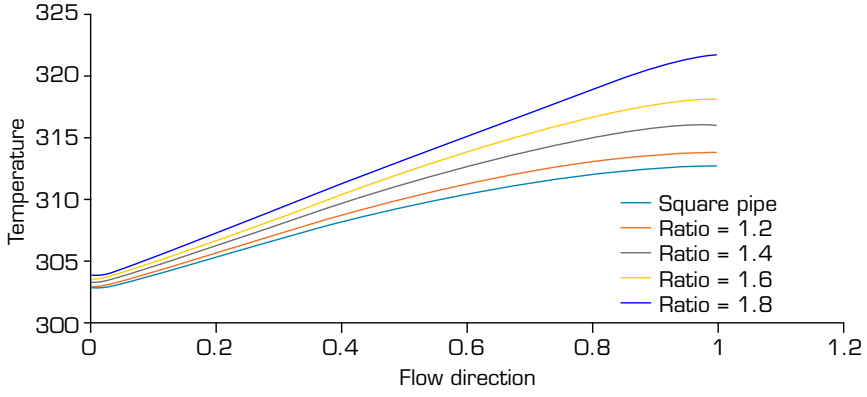

Source: ANSYS analysis.

Figure 13. Temperature distribution for different expansion ratios in the case of expanded both vertical and horizontal sides.

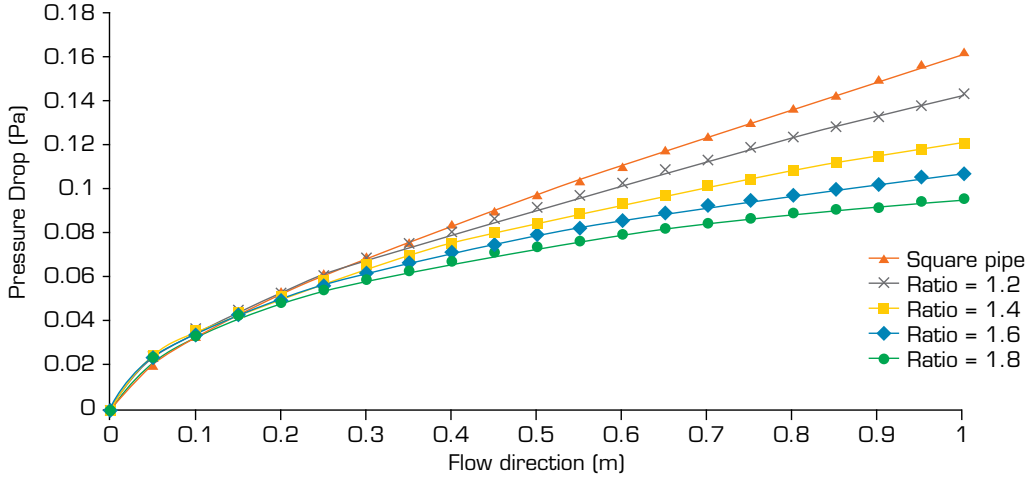

Source: ANSYS analysis.

Figure 14. Pressure drop with the flow direction in the case of expanded vertical sides for different expansion ratios.

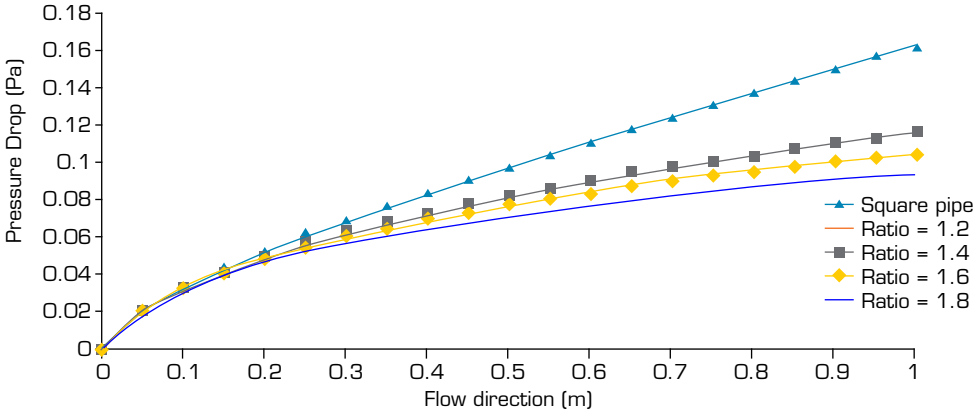

Source: ANSYS analysis.

Figure 15. Pressure drop with the flow direction in the case of expanded horizontal sides for different expansion ratios.

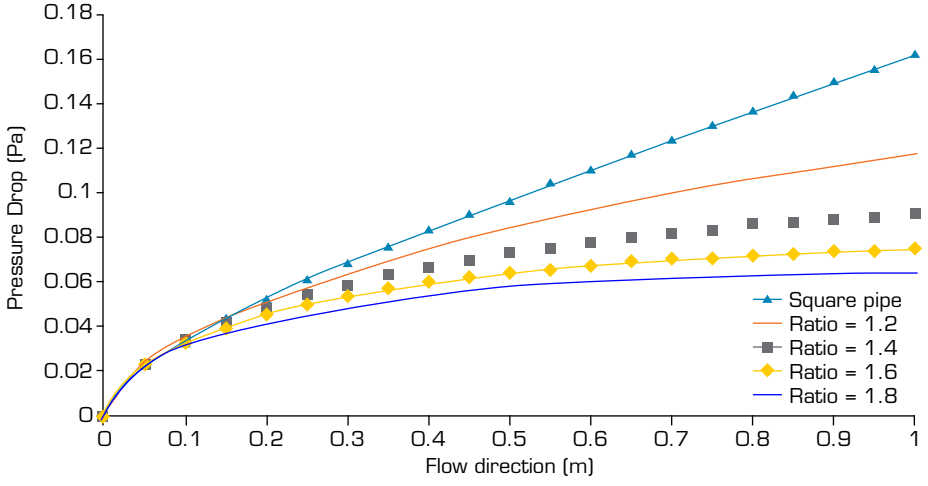

Source: ANSYS analysis.

Figure 16. Pressure drop with the flow direction in the case of all sides expanded for different expansion ratios.

Figures 17-19 show the temperature difference between pipe inlets to pipe exit at all cases under study at different expansion ratios. It is so obvious that the third case records maximum temperature difference percentage reaches to 45.5%. This means the third case witnessed a maximum heat transfer rate because of the larger area if it compared with previous two cases.

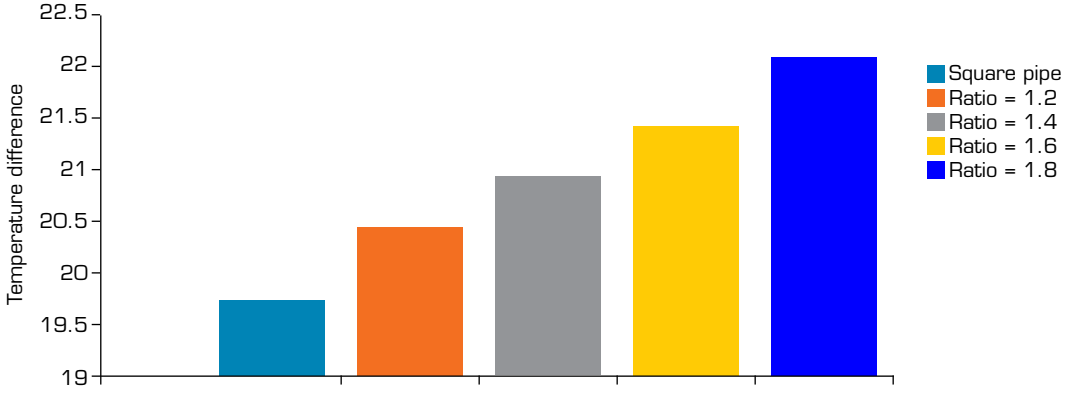

Source: ANSYS analysis.

Figure 17. Temperature difference along flow direction for different expansion ratios in the case of expanded vertical sides.

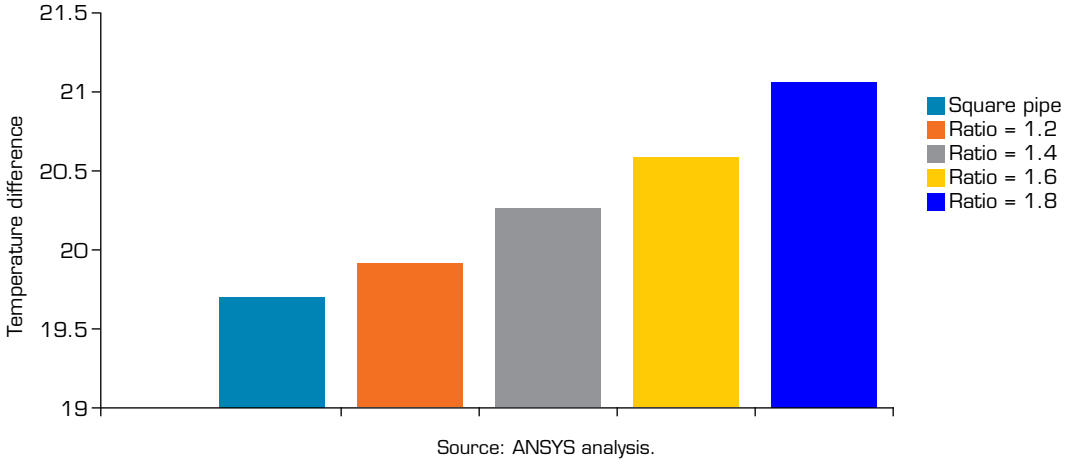

Source: ANSYS analysis.

Figure 18. Temperature difference along flow direction for different expansion ratios in the case of expanded horizontal sides.

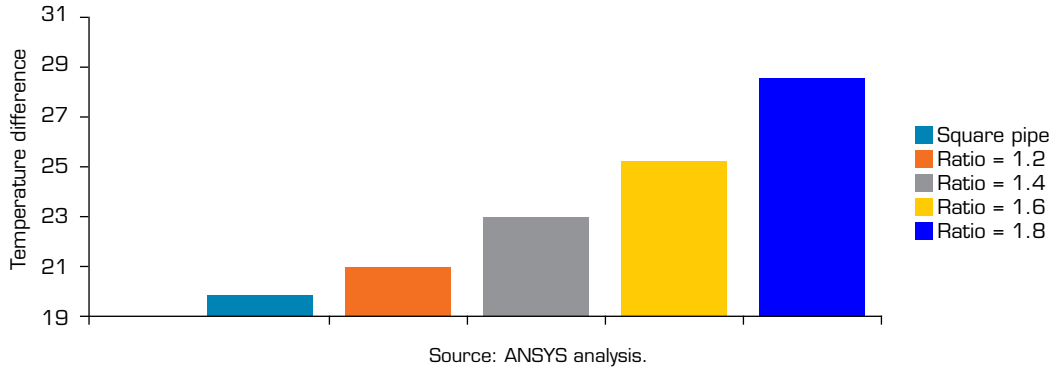

Source: ANSYS analysis.

Figure 19. Temperature difference along flow direction for different expansion ratios in the case of expanded both vertical and horizontal sides.

Figures 20-22 show the values of hydraulic-thermal performance function ratio in all cases under study for all studied expansion ratios. As the expansion ratio increases, the area increases, which means the heat transfer phenomena enhances, then the hydraulic ratio increases. The maximum increase occurs at third case, when the expansion ratio reaches to 1.8.

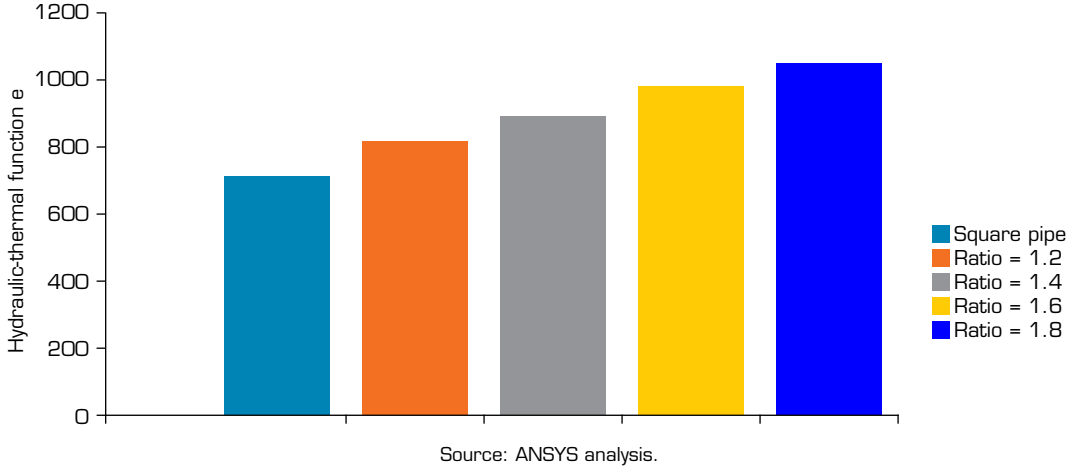

Source: ANSYS analysis.

Figure 20. Hydraulic-thermal performance function for different expansion ratios in the case of expanded vertical sides.

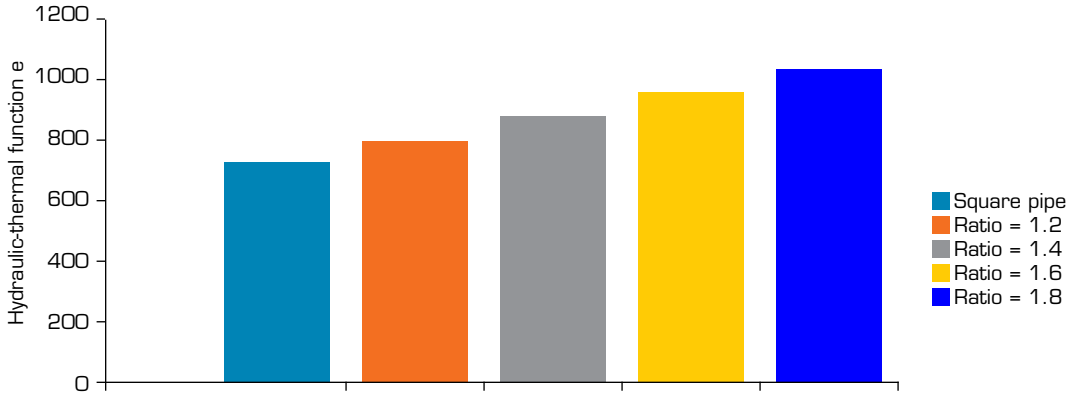

Source: ANSYS analysis.

Figure 21. Hydraulic-thermal performance function for different expansion ratios in the case of expanded horizontal sides.

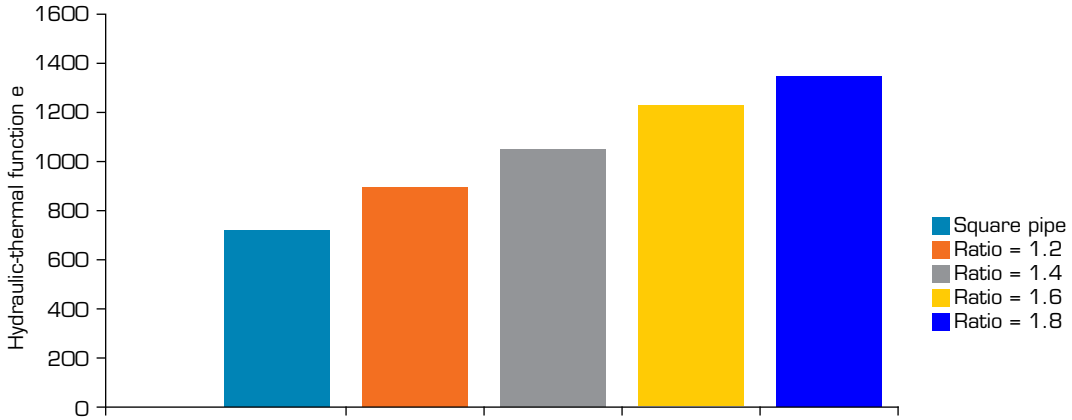

Source: ANSYS analysis.

Figure 22. Hydraulic-thermal performance function for different expansion ratios in the case of all sides expanded.

In Table 1, the ratio of the hydraulic-thermal performance functions for each case to the same function in the case of square pipe is presented. In the first two cases, there are no large significant changes (the total area remains constant). In the third case, a noticeable increase is observed, with the area doubling. Consequently, the heat transfer significantly improves, reaching an enhancement of 48%.

Table 1. The ratio of hydraulic-thermal performance functions in each case at different expansion ratio to the hydraulic-thermal performance functions of square pipe.

Cases	Ratio			
	1.2	1.4	1.6	1.8
Vertical sides expansion at exit	114.327	126.135	137.081	146.689
Horizontal sides expansion at exit	110.172	123.137	134.367	144.325
Both vertical and horizontal sides expansion	125.525	147.996	172.455	186.845

Source: ANSYS analysis.

CONCLUSIONS

By analyzing the heat transfer phenomena and the pressure drop through the cases under study, it can be concluded that:

- A maximum temperature difference of 45.5% can be recorded if all sides are expanded at the outlet at a ratio of 1.8;
- The enhancement in pressure drop reaches to 153% at a ratio of 1.8 in the third case. As a result, the hydraulic-thermal performance function is increased by 48%.

CONFLICT OF INTEREST

Nothing to declare.

AUTHORS' CONTRIBUTION

Conceptualization: Ahmed SS; **Methodology:** Hashim NA, Ahmed SS; **Software:** Ahmed SS, Hashim NA; **Validation:** Hashim RH, Al-Fatlwe FMK; **Formal analysis:** Ahmed SS; **Investigation:** Hashim NA; **Resources:** Al-Fatlwe FMK; **Data Curation:** Hashim NA, Ahmed SS; **Writing - Original Draft:** Hashim NA; **Writing - Review & Editing:** Ahmed SS; **Final approval:** HashimNA.

DATA AVAILABILITY STATEMENT

Data sharing is not applicable.

FUNDING

Not applicable.

ACKNOWLEDGMENTS

Not applicable.

REFERENCES

Barnoon P, Toghraie D, Dehkordi R, Afrand M (2019) Two phase natural convection and thermal radiation of non-newtonian nanofluid in a porous cavity considering inclined cavity and size of inside cylinders. Int Commun Heat Mass Transf 108:e104285. http://doi.org/10.1016/j.icheatmasstransfer.2019.104285

Bashir AI, Everts M, Bennacer R, Meyer JP (2019) Single-phase forced convection heat transfer and pressure drop in circular tubes in the laminar and transitional flow regimes. Exp Therm Fluid Sci 109:e109891. http://doi.org/10.1016/j.expthermflusci.2019.109891

Gheynan AR, Akbari OA, Zarringhalam M, Shabani GA, Sheikh AAA, Goodarzi M, Toghraie D (2019) Investigating the effect of nanoparticles diameter on turbulent flow and heat transfer properties of non-newtonian carboxymethyl cellulose/CuO fluid in a microtube. Int J Numer Methods Heat Fluid Flow 29(5). http://dx.doi.org/10.1108/HFF-07-2018-0368

Kakac S, Shah R, Aung W (1987) Handbook of single-phase convective heat transfer. New York: John Wiley and Sons.

Laila R, Nawaz D, Marwat K, Ali A (2021) Flow and heat transfer in a rectangular converging (diverging) channel: new formulation. J Egypt Math Soc 29(18). http://doi.org/10.1186/s42787-021-00126-7

Lee MS, Jeong SS, Ahn SW, Han JC (2013) Heat transfer and friction in rectangular convergent and divergent channels with ribs. J Thermophys Heat Transf 27(4):660–667. http://doi.org/10.2514/1.T4144

Mashaei RP, HosseinSM, Bahiraei M (2012) Numerical investigation of nanofluid forced convection in channels with discrete heat sources. J Appl Math e:259284. http://doi.org/10.1155/2012/259284

Massoud M (2007) Engineering thermofluids. Thermodynamics, fluid mechanics, and heat transfer. Boston: Springer.

Negi P, Kalra J, Subhash M (2019) Effect (KN and RE) on performance index of concentric circular micro channel. International Journal of Innovative Technology and Exploring Engineering 8(10). http://doi.org/10.35940/ijitee.J1012.08810S219

Patel A, Namjoshi S, Singh SK (2005) Comparative thermal performance evaluation of U Tube and straight tube solar water heater. International Journal of Research in Engineering and Science 1(6):346-352.

Salih SM, Yaseen DT (2021) Numerical modeling of laminar forced convective enhancement of (AL_2O_3-Water) nano fluid in a circular pipe. Kufa Journal of Engineering 11(4)19-30.

Shah RK, London AL (1980) Effects of nonuniform passages on compact heat exchanger performance. J Eng Gas Turbines Power 102(3):653-659. http://doi.org/10.1115/1.3230319

Srivastava P, Dewan A, Bajpai JK (2017) Flow and heat transfer characteristics in convergent-divergent shaped microchannel with ribs and cavities. Int J Heat Technol 35(4):863-873. http://doi.org/10.18280/ijht.350423

Toghraie D (2017) The investigation of simultaneous heat transfer of water/Al 2 O 3 nanofluid in a close enclosure by applying homogeneous magnetic field. Int J Mech Sci 133:674-688. http://doi.org/10.1016/j.ijmecsci.2017.09.035

Vahidifar S, Kahrom M (2015) Experimental study of heat transfer enhancement in a heated tube caused by wire-coil and rings. J Appl Fluid Mech 8(4):885-892. http://doi.org/10.18869/acadpub.jafm.67.223.23359

Webb RL, Kim NY (2005) Principle of enhanced heat transfer. 2nd ed. New York: Taylor and Francis.